Ryberg, T., Weber, M. (2000): Receiver function arrays: a reflection seismic approach. - Geophysical Journal International, 141, 1, pp. 1—11.

DOI: https://doi.org/10.1046/j.1365-246X.2000.00077.x

Geophys. J. Int. (2000) **141,** 1–11

Receiver function arrays: a reflection seismic approach

T. Ryberg and M. Weber
GeoForschungsZentrum, Telegrafenberg, 14473 *Potsdam, Germany. E-mail: trond@gfz-potsdam.de*

Accepted 1999 September 10. Received 1999 August 18; in original form 1999 March 29

SUMMARY

The receiver function method (RFM) is a commonly used technique to study the crustal and upper mantle velocity structure. Early receiver function (RF) investigations were performed mostly at individual permanent stations. They were focused on crustal structures, and later on upper mantle velocity discontinuities (410 km and 660 km discontinuities). Only recently has research been directed towards the study of the lateral (2- and 3-D) variability of major velocity boundaries in the crust and upper mantle by receiver function arrays using temporary and permanent, three-component, short-period and broad-band seismic stations. To improve the signal-to-noise ratio, receiver functions are calculated for individual earthquakes and are then binned, moveout corrected and stacked. We show that this processing sequence is similar to that applied routinely in exploration seismology. Therefore, existing tools from the near-vertical data processing can be adopted for receiver functions: velocity analysis tools, solutions for static and residual static problems, coherence enhancement of seismic phases, migration, etc. The high spatial density of seismic stations of recent and future receiver function experiments provides the opportunity (and obligation) to use the more sophisticated migration methods (full wavefield migration) commonly and successfully used in exploration seismics.

Synthetics calculated by the finite difference method for simple 2-D crustal models are employed here to test our processing approach and to show the potentials and limitations of stacking and migrating RF data. We show that binning, normal moveout (NMO) corrections, stacking and post-stack migration of the synthetic data can reconstruct the models reliably with a high spatial resolution.

Key words: crustal structure, finite difference methods, reflection seismology, seismic wave propagation, synthetic seismograms.

1 INTRODUCTION

The receiver function method (RFM) is a commonly used technique to study the crustal and upper mantle velocity structure using temporary and permanent, three-component, short-period and broad-band seismic stations. While early receiver function investigations were mostly performed with individual permanent stations (Burdick & Langston 1977; Langston 1977, 1979; Vinnik 1977) and focused mainly on crustal structures, only recently has much research been successfully directed towards studying the lateral (2- and 3-D) variability of major velocity boundaries in the crust and upper mantle by receiver function arrays. At present more and more 1- and 2-D arrays of short-period and broad-band stations are being temporarily deployed to image the Moho, 410 and 660 km discontinuities (Hedlin *et al.* 1994; Revenaugh 1995; Dueker & Sheehan 1997; Bostock 1998; Peng & Humphreys 1998; Kosarev *et al.* 1999). The data are used to derive images of the upper mantle and crust by investigating the *PS* conversions and *S*-wave reverberations caused by major velocity discontinuities.

To improve the signal-to-noise ratio, receiver functions obtained for individual earthquakes are binned, moveout corrected and subsequently stacked. The standard procedure of processing receiver functions consists of the following steps (Langston 1977; Vinnik 1977). First, the seismograms are rotated from the vertical/horizontal to the *LQT* coordinate system (in an attempt to separate the *P*, *SV* and *SH* energy) (Yuan *et al.* 1997). This step is followed by a deconvolution to remove the effect of different source time functions. A moveout correction is then applied to the data to remove the kinematic effect of different earthquake distances before stacking individual receiver functions. This data processing procedure is similar to

that applied routinely in exploration seismology. Therefore, it is appropriate to adapt and modify the existing tools used in near-vertical data processing to the needs of receiver functions, so that we can take advantage of state-of-the-art exploration seismic tools. Instead of taking the two-way traveltime and the *P*-wave velocity as in exploration we have to replace them by the one-way traveltime and the *S*-wave velocity, respectively. When we analyse mainly converted phases we have to substitute the term reflector by the term 'convertor'. Although there are differences between these techniques, we can easily adapt most of the tools applied in exploration seismology, for example, velocity and depth analysis tools [velocity spectrum stacks (VSS) of Gurrola *et al.* (1994) and Gurrola & Minster (1998)], solutions for static and residual static problems, coherence enhancement of seismic phases, and migration (Bostock & Rondenay 1999).

The lateral variability of lithospheric boundaries has been studied using 1- and 2-D arrays of short-period and broad-band seismic stations. Depending on the density of station spacing and the frequency content of the recorded waves, different processing techniques have been applied to the individual receiver functions. The spectrum of techniques starts from analysing and stacking of RF from individual stations, analysing the waveforms to obtain 1-D velocity functions, plotting them side by side (Kosarev *et al.* 1999; Peng & Humphreys 1998) and goes on to the binning and stacking of receiver functions (Yuan *et al.* 1997; Dueker & Sheehan 1997, 1998; Bostock 1998). To obtain more precise images of the lithospheric boundaries, the technique of stacking receiver functions along back-projected rays has been used successfully (Jones & Phinney 1998; Kosarev *et al.* 1999; Gossler *et al.* 1999). Details of this procedure can be found in Jones & Phinney (1998). While the latter methods try to image the boundaries at their true location by back-projecting the traces, these methods will not be able to image scattered (direct *PP* and converted *PS*) energy correctly, because none of them applies full wavefield migration. The previous methods represent high-frequency approximations of the imaging process because they assume that all energy propagates along rays; it is consequently mapped along them. The diffracted energy is mapped to incorrect locations, and diffraction hyperbolae cannot be collapsed using this stacking technique. The relatively low spatial density of observational points justifies the application of these relatively simple migration methods; they result in lithospheric images with better accuracy than images constructed of RF traces simply plotted side by side. However, the high spatial density of seismic stations of recent (Dueker & Sheehan 1998; Gossler *et al.* 1999) and future experiments now gives the opportunity to apply the more sophisticated and better migration methods (e.g. full wavefield migration) commonly and successfully used in exploration seismics (Yilmaz 1987; Sheriff & Geldart 1995). Unmigrated stacked sections have the theoretically limited horizontal resolution described by the Fresnel zone (Yilmaz 1987; Sheriff & Geldart 1995). Only with the application of migration methods can one increase the horizontal resolution approaching the theoretical limit of $\lambda/2$, assuming that high-quality and sufficiently dense data sets (receiver- and source-related) are available. Recently, Bostock & Rondenay (1999) suggested a processing method that treats all *P*-wave coda energy as being caused by scatterers. It focuses on the decomposition of the recorded wavefield into direct (source and multiples) and converted (scattered) components. After extraction of the source wavelet the remaining energy is interpreted as scattered energy and could be successfully migrated exploiting a single-scattering (Born) concept.

In this paper synthetic seismograms calculated for laterally varying structures have been processed by the RFM. We perform binning, stacking and post-stack depth migration to reconstruct our input models. For the sake of clarity we limit our analysis to noise-free synthetic data for several simple 2-D crustal models and to post-stack depth migration instead of its pre-stack version. We are aware of the problems of not applying pre-stack migration to our synthetics and suggest that for real data of high enough quality, pre-stack migration should also be applied. We study the influence of non-ideal receiver spacings and source distributions, and the influence of the *a priori* unknown velocity model on the imaging capabilities. We show that migration is especially crucial to imaging correctly dipping discontinuities and complicated structures. Synthetics calculated by the finite difference method for simple 2-D models show in addition to the converted phases relatively strong *P*-wave energy on the *Q* component and, as expected, strong *P* and *S* diffractions. The application of the Kirchhoff depth migration technique images the true position of the convertors and collapses the *S*-wave diffraction hyperbolae, resulting in a significant improvement of the imaging potential of the RFM.

2 MOVEOUT CORRECTION, BINNING AND STACKING

To demonstrate the kinematic equivalence of the reflection of a *P* wave at near-vertical incidence in exploration seismics and the *PS* conversion at boundaries for teleseismic events we take the case of a flat reflector at depth Z overlain by a constant-velocity (V_P) layer (see Fig. 1).

For this case the two-way traveltime of the reflected wave is given by

$$T_{\mathrm{TWT}} = \frac{1}{V_P}\sqrt{X^2 + 4Z^2}\,, \tag{1}$$

where X is the distance between source and receiver (Yilmaz 1987; Sheriff & Geldart 1995). This is the well-known expression for a reflection traveltime hyperbola,

$$T_{\mathrm{TWT}}^2 = \frac{X^2}{V_P^2} + \frac{4Z^2}{V_P^2}\,. \tag{2}$$

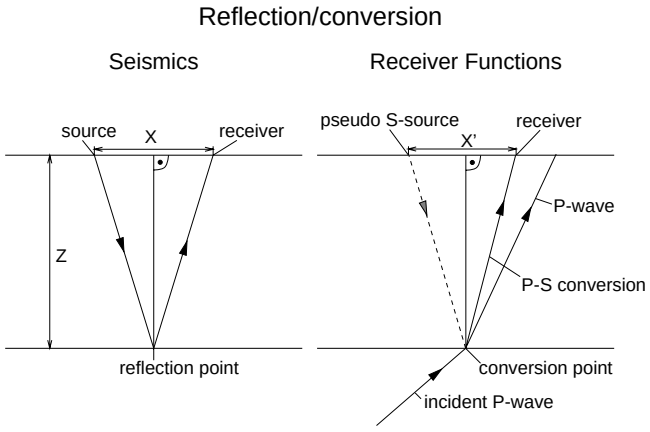

Figure 1. Sketch showing the equivalence of the near-vertical reflection and the conversion.

In the case of small incidence angles (or equivalent true distances in the case of near-vertical data) the following approximation [small-spread approximation in exploration seismics (Yilmaz 1987)] holds and eq. (1) can be rewritten as

$$T_{\mathrm{TWT}} = \frac{2Z}{V_P} + \frac{X^2}{4ZV_P} + O(X^4)\,. \tag{3}$$

Assuming a plane *P* wave incident from below at an interface at depth Z, we obtain the delay time between *P* and the *PS* converted phase at that interface:

$$T_{PS} = Z\left(\sqrt{V_S^{-2} - p^2} - \sqrt{V_P^{-2} - p^2}\right), \tag{4}$$

where p is the ray parameter, and V_P and V_S are the *P*- and *S*-wave velocities, respectively (Gurrola *et al.* 1994). A simple transformation under the assumption of small p yields

$$T_{PS} = Z(V_S^{-1} - V_P^{-1}) + \frac{Z(V_P - V_S)p^2}{2} + O(p^4)\,. \tag{5}$$

By comparing the coefficients in eqs (3) and (5) we can define a 'new' pseudo-velocity, V':

$$V' = \frac{2V_S V_P}{V_P - V_S}\,, \tag{6}$$

and a pseudo-distance, X':

$$X' = \sqrt{V_P/V_S}\, V_S\, 2pZ\,. \tag{7}$$

The pseudo-distance X' can be rewritten as

$$X' = \sqrt{V_P/V_S}\, X_s \sqrt{1 - p^2 V_S^2} \simeq \sqrt{V_P/V_S}\, X_s\,, \tag{8}$$

with $X_s = 2pV_S Z$ being the distance from the receiver to the position of a pseudo-*S*-wave surface source with a reflection point at the same location as that where the conversion occurs (see Fig. 1). The small-spread approximation in exploration seismics (Yilmaz 1987) is equivalent to small p, or pseudo-distances X' or X_s in the case of the RFM.

As in standard near-vertical reflection seismics, traces from different earthquakes (sources) have to be moveout corrected before stacking. To do this, all traces with common conversion (CCP) or piercing points, or with conversion points falling in a given bin have to be selected, similar to the common depth point sorting (CDP) used in exploration seismics. Now that the traveltimes of a reflector for near-vertical reflections and *PS* conversions are equivalent, the standard procedure of moveout corrections can be applied to produce zero-offset traces (zero source–receiver or pseudo-source–receiver distances). The zero-offset traces in near-vertical seismics are hypothetical traces with source and receiver at the same place. The moveout correction of receiver functions to a zero pseudo-source–receiver distance (hypothetical antipode earthquake, or $p = 0$) is equivalent to the case of perpendicular *P*-wave incidence. It is interesting that normal incidence of a *P* wave on a plane boundary would, of course, not produce a *PS* conversion. However, because the moveout correction is a kinematic correction, these converted waves do not disappear. To enhance the signal-to-noise ratio, traces with the same reflection/conversion points can be subsequently stacked. It is important to note that the traveltimes for waves from a reflector eq. (3) and a convertor eq. (5) are described by similar equations. The dynamic behaviour (amplitude distribution versus offset) differs due to different reflection and conversion coefficients and also due to different recording coordinate systems (vertical components in reflection seismics, *Q* components for *PS* conversions). For instance, vertical incidence of *P* waves will produce reflections, but no conversions. Earthquakes used for receiver function studies cover the distance range 80°–23°, equivalent to *P*-wave incidence angles at the Moho in standard earth models such as IASP91 (Kennett & Engdahl 1991) ranging from 23° to 37°. These incidence angles correspond to the near-vertical incidence case of exploration seismics with respect to the small-spread approximation in exploration seismics (Yilmaz 1987).

Now that the equivalence of near-vertical seismic processing and the receiver function method has been shown, it is an obvious move to apply other highly effective data processing tools commonly used in exploration seismics. One typical problem in exploration seismics is the *a priori* unknown subsurface velocity structure, which has to be used to calculate and apply normal moveout (NMO) corrections before stacking. For a typical crustal structure with a Moho at 30 km depth and earthquakes routinely used to study RF, one can expect only small moveouts of the order of several hundred milliseconds. Upper mantle discontinuities yield moveout times of several seconds. Using NMO velocity analysis tools [constant velocity stacks, semblance analysis, etc.; see also Gurrola *et al.* (1994)], optimum velocity functions can be derived from the data, resulting in high-quality stacked images. The success of this approach relies strongly on the existence of convertors (boundaries) with amplitudes above the background noise. In addition to these analytical time shifts (NMO), other remaining time delays can be handled by static analysis tools and residual static data processing. Signal-to-noise ratios can be further improved by coherence enhancement processing steps.

3 MIGRATION

To study more complex models with receiver functions, migration, that is, the method to image the true position of convertors, becomes an important issue. A simple assumption would be that a complex model is constructed of individual points, each acting as a Huygens' secondary source (both a *P*- and an *S*-wave source simultaneously). The superposition of all secondary sources (point diffractors) will result in the wavefield recorded at the surface. Reversing this process will result in a depth-migrated image, with all diffractors at their true positions.

To demonstrate the equivalence of the migration principle used in conventional seismics and the receiver function method, we limit our considerations for the sake of clarity to the 2-D case of a point diffractor embedded in a homogeneous half-space and assume NMO-corrected and stacked data (zero-offset case) (see Fig. 2).

The traveltime equation of the diffraction hyperbola in reflection seismics is given by

$$T_{\mathrm{TWT}} = \frac{2}{V_P}\sqrt{X_{\mathrm{D}}^2 + Z^2}\,. \tag{9}$$

The traveltime for a *PS* diffraction for a stacked section (vertically incident *P* wave, conversion to an *S* wave, see Fig. 2)

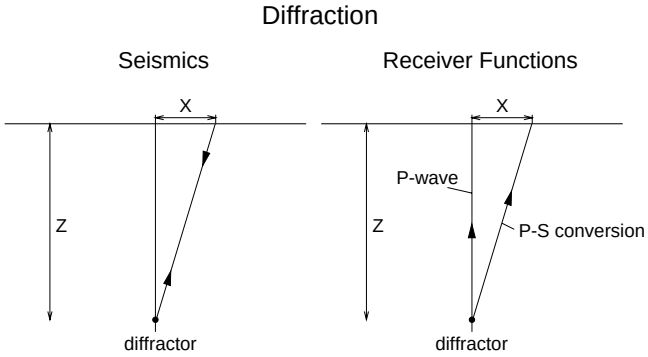

Figure 2. Sketch showing the geometry of the diffracted phases for the near-vertical reflection (left) and the conversion (right) cases for zero-offset traces; X_d is the horizontal distance to the diffractor.

can be written as

$$T_{PS} = \frac{1}{V_S}\sqrt{X_D^2 + Z^2} - \frac{Z}{V_P}, \tag{10}$$

where the first part describes the time related to the *S* phase. The second part is caused by the fact that the traveltime of the converted phase is given relative to the direct (not diffracted) *P* wave. Obviously, this is an equation of a time-shifted hyperbola and can therefore be written as

$$T_{PS}^* = T_{PS} + \frac{Z}{V_P} = \frac{1}{V_S}\sqrt{X_D^2 + Z^2}. \tag{11}$$

This equation is that of a diffraction hyperbola, similar to eq. (9),

$$T_{PS}^* = \frac{2}{V_d^*}\sqrt{X_D^2 + Z^2}, \tag{12}$$

with the 'new' diffraction velocity

$$V_d^* = 2V_S. \tag{13}$$

Note that not only a *S*-phase diffraction hyperbola will be present in the data but also a *PP* diffraction will occur, travelling just behind the incident *P* wave and with a specific moveout (see Fig. 3). In unmigrated stacked receiver function sections, point diffractors will be imaged as diffraction hyperbolae similar to the near-vertical seismic case. Migration after time-shifting will therefore collapse hyperbolic events to their appropriate point structures.

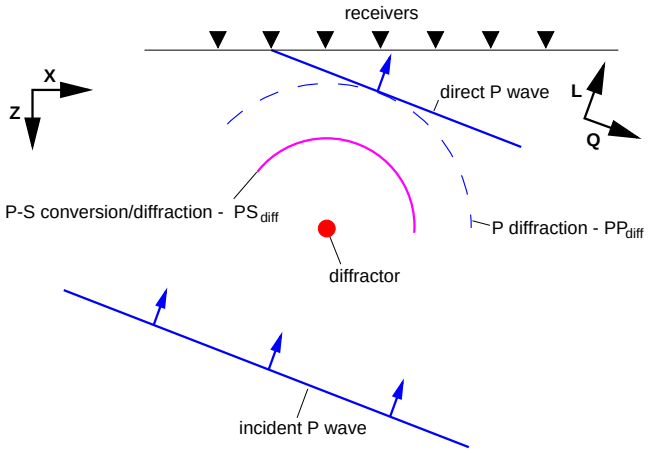

Figure 3. Sketch showing the phases generated by a point diffractor for plane *P*-wave incidence. The ray coordinate system (L, Q) is also given.

Similar to the near-vertical incidence scenario for the case of a reflector, we can describe the traveltime for the respective convertor/diffractor. There is of course a difference in the amplitude distribution due to the different scattering of an incident *P* wave into *P* and *S* waves (Wu & Aki 1985) and the fact that the receivers record different components of the wavefield. Due to the rotation from the *ZX* to the *LQ* coordinate system there will be some *PP* diffraction energy on the *Q* component and some *PS* diffraction energy on the *L* component. For the simple models used in this paper, post-stack depth migration is sufficient to reconstruct the input models. Of course, for more complicated models and observed data, pre-stack migration techniques have to be applied to obtain correct crustal images.

4 MODELLING AND STACKING OF SYNTHETIC SEISMOGRAMS

To test the application of the suggested processing steps we calculated complete synthetic seismograms using the finite difference method (Kelly *et al.* 1976). We calculated synthetics for 2-D crustal models consisting of a simple point scatterer embedded in a homogeneous half-space, a crustal model with a Moho step (kink model), a Moho dome and a flat Moho model overlain by a basin structure (Fig. 4, models a, b, c and d). In these models the *S*-wave velocity and the density were chosen to be correlated to the *P*-wave velocity via the often used $\sqrt{3}$ relation and Birch's law (Birch 1961), respectively.

We simulated earthquakes with plane *P* waves impinging on the Moho with incidence angles ranging from 23° to 37° (15 steps). This is equivalent to teleseismic *P* arrivals with ray parameters from 0.048 to 0.075 s km^{-1} (epicentral distances from 23° to 80°). The dominant frequency of the wavelet is 1 Hz. Fig. 5 shows two snapshots of the vertical and horizontal components for the interaction of a plane wave arrival from the left with the kink model. These snapshots give a good representation of the complexity of the wavefield for this very simple model. The snapshots are characterized by strong direct *P* waves, their conversion at the Moho boundary, and a complex wavefield consisting of *PP* and *PS* scattered phases.

This calculation and those for the other models was followed by the standard procedure of rotation of the vertical- and horizontal-component seismograms into an *LQ* coordinate system parallel and perpendicular to the incident *P*-wave motion at the surface (Yuan *et al.* 1997). The seismograms have been time-aligned with respect to the first *P* onset. Fig. 6 shows two examples of the plane wave response of two models. Both record sections (time-aligned *Q* components) are dominated by the *PS* conversions and *PP* diffractions.

Note that the *PS* and *PP* diffractions have similar amplitudes on the *Q* components. Our aim was not to test the effectiveness of the deconvolution process needed to correct the seismograms for different sources in real data. We therefore calculated relatively broad-band synthetics (short wavelets), and no noise was added to the synthetics.

Synthetic data from 30 plane wave simulations (representing 15 earthquakes from both the left and right sides) recorded at the surface have been time-aligned on the first *P* arrivals,

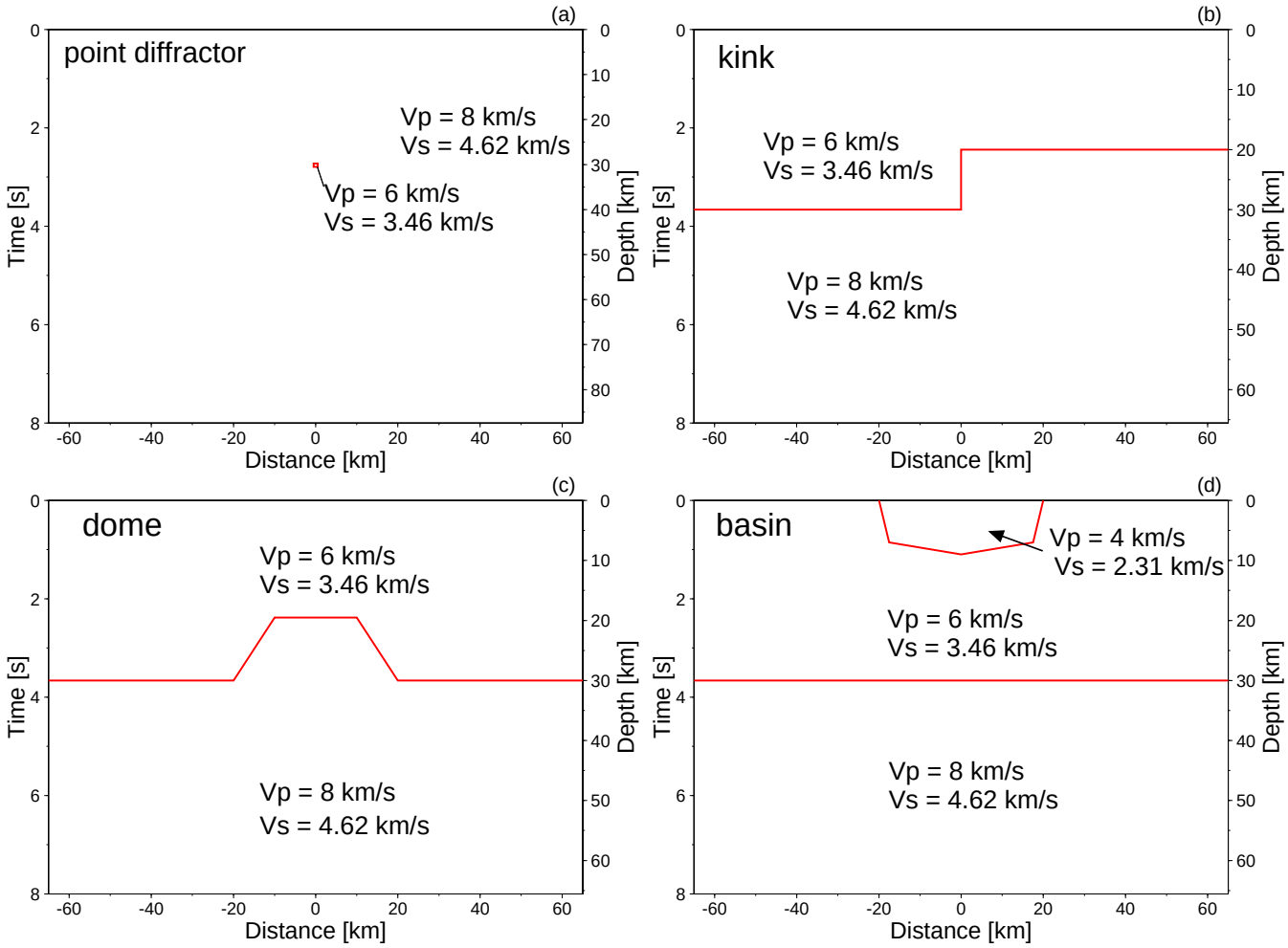

Figure 4. Crustal models studied. Model (a) is a point diffractor embedded in a homogeneous half-space; models (b), (c) and (d) represent simple crustal models. In addition to the depth scale, an approximate timescale is added. The *S*-wave velocities have been derived by the $\sqrt{3}$-relation.

rotated and binned (sorted for common conversion points—CCP for the four models of Fig. 4). After this sorting, the NMO correction was determined by a standard velocity analysis of the data using constant-velocity stacks similar to Gurrola *et al.* (1994). Not too surprisingly, the correct NMO velocities are identical to those predicted by eq. (6). Consequently, the NMO corrected data could be stacked to recover the crustal images. Fig. 7 (left panels) shows the CCP stacked images for the point diffractor and the kink, dome and basin models.

5 MIGRATION OF SYNTHETIC SEISMOGRAMS

A comparison of the input models with the stacked sections shows systematic differences. Instead of resulting in a point-like structure, the point diffractor image is similar to a diffraction hyperbola. Similar diffractive phases can be seen for all the other stacked images. Especially strong artefacts are seen in the stacked section for the basin model at larger depths. These phases represent multiply reflected (and/or converted, diffracted) phases from within the basin. They can be misinterpreted because although they are caused by shallow structures, they appear at larger times/depths. These complications caused by thick sedimentary basins due to mode conversions and multiples, which tend to degrade the receiver functions, have also been mentioned by Levander & Hill (1985) and Dueker & Sheehan (1998). Note also the apparent time delay of the Moho due to the low-velocity sediments above it. Additionally, all CCP stacked sections have relatively strong artefacts at shallow depths (small traveltimes) caused by *PP* diffraction at deeper structures (see Fig. 6 for details). All stacked sections have low horizontal resolutions as one would expect taking into account the appropriate Fresnel zone (Saunders *et al.* 1998). The diameter of the first Fresnel zone is defined as

$$D_{\mathrm{F}} = \sqrt{2ZTV + \frac{T^2 V^2}{4}} \tag{14}$$

(Yilmaz 1987), where Z is the depth to the boundary, T is the period of the signal and V is the appropriate medium velocity. For a 30 km deep Moho, a crustal S wave velocity of 3.46 km s^{-1} and a typical frequency of 1 Hz, the first Fresnel zone is of the order of 15 km.

Waveform migration is necessary to image the crustal structures correctly, to 'collapse' the diffraction hyperbolae and to improve the horizontal resolution (that is, to overcome the Fresnel zone limitation). From near-vertical seismic data processing it is well known that depth migration is essential

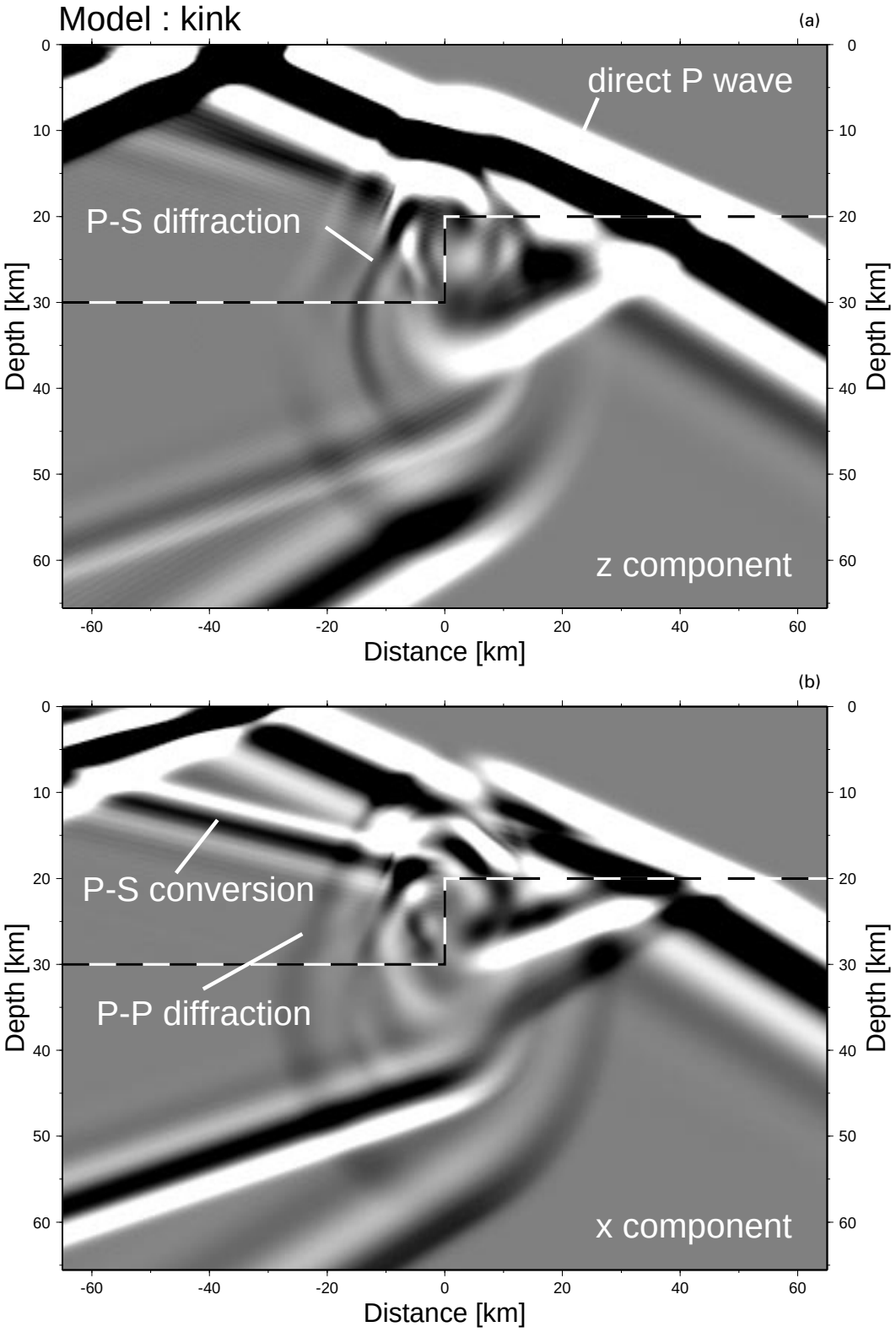

Figure 5. Snapshots of the wavefield for a plane *P* wave impinging on the kink model (Fig. 4b) from the left at an angle of 23°. The *Z*- and *X*-component wavefields (a and b) show the complex wavefield of several converted and diffracted waves. The dominant frequency of the wavelet is 1 Hz.

for imaging dipping reflectors/convertors correctly. Going one step further than Jones & Phinney (1998), Kosarev *et al.* (1999) and Gossler *et al.* (1999), who migrated (imaged) receiver functions along curved ray paths, we use true waveform migration techniques. As our velocity models are relatively simple, we choose the post-stack Kirchhoff depth migration. If we consider the time shift according to eq. (11) and use the migration velocity taken from our input models, we can

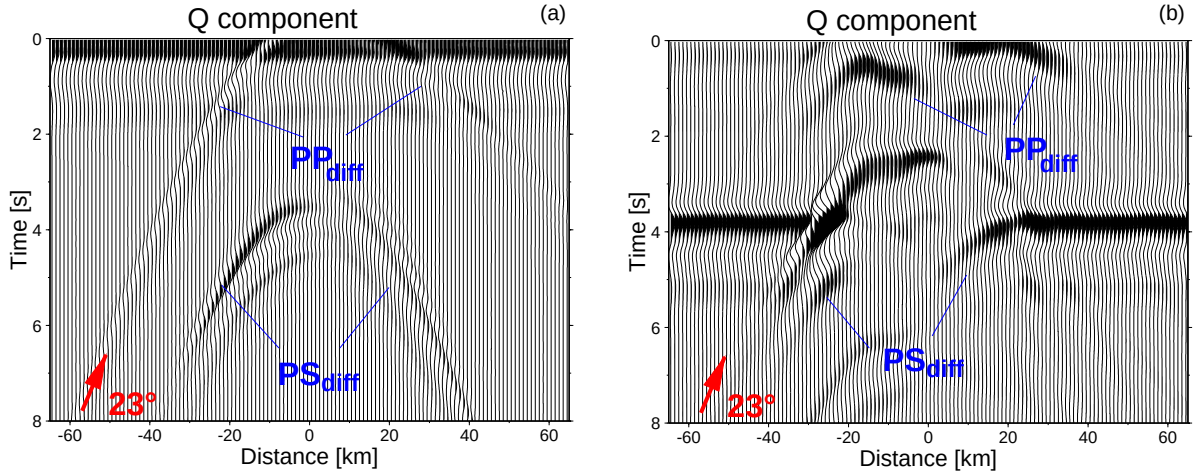

Figure 6. Time-aligned *Q*-component seismograms for model (a) (left) (point diffractor) and model (c) (right) (dome) for a plane wave incident at an angle of 23°. The receiver spacing is 1 km. Several converted and diffracted arrivals are labelled. Note the existence of a small-amplitude side lobe travelling 1.5 s behind the main signal due to the bandlimited character of the source wavelet.

migrate the CCP stacked section using the Kirchhoff depth migration (Yilmaz 1987). We replaced the migration velocity V_P of zero-offset migration by $V_d^* = 2V_S$ according to eq. (13). Fig. 7 (right panels) shows the migrated images for the point diffractor, the kink, the dome and the basin models for a migration with the correct velocities. The comparison with the unmigrated sections (left panel) demonstrates the significant improvement of the images. The diffraction hyperbola migrates to an almost point-like structure of the point scatterer. Similarly for the other models, the diffraction hyperbolae are strongly suppressed and collapsed to the appropriate structures. In particular, the *PP* diffraction hyperbolae are greatly suppressed. Although some migrational noise has been introduced, the overall signal-to-noise ratio is improved significantly.

A general problem in near-vertical seismic data processing is that the migration velocity model is usually unknown and must be derived from boreholes, the NMO velocity analysis, or other geophysical methods. To test the sensitivity of the migration scheme employed here we migrated the point and dome model with slightly incorrect velocity models. Fig. 8 shows the depth-migrated sections with background velocity models characterized by reduced and increased (by 10 and 20 per cent) velocities with respect to the true velocities.

Although some defocusing occurs, even a velocity incorrect by 10 per cent will result in a reasonable migration result. Migration with velocities incorrect by more than 10 per cent results in poor images. This shows that even a migration with incorrect velocities is generally better than using the unmigrated image. One exception is the basin model in Fig. 8, lower right. The existence of shallow structures with different velocities will greatly reduce the capability of imaging deeper structures correctly. Probably, internal multiples, multiple conversions and strong diffractions have a great impact on the image of deeper structures, limiting the possibilities of using receiver functions to image structures overlain by sedimentary units [similar problems have been reported by Levander & Hill 1985) and Dueker & Sheehan (1998)].

Up to now we have assumed a constant receiver spacing of only 1 km. The other idealistic assumption was the perfect distribution of earthquakes (15 from each side) covering the whole distance range usable in the RFM. In reality such a situation has not been achievable with past and current field experiments. To simulate a more realistic scenario we took random subsets of our data, reducing the average station spacing to 2, 5 and 10 km. We applied the binning, NMO corrections, stacking and post-stack depth migration as described before. Figs 9(a)–(d) show the migrated sections for average receiver spacings of 1, 2, 5 and 10 km.

While station spacings of 2 and 5 km can still recover the input model (dome), station spacings larger than 5 km result, even under these still ideal conditions (identical earthquakes, no noise, etc.) in a very poor reconstruction of the dome. Similar degradation effects are expected for non-ideal source (earthquake) distributions. To test the capabilities of reconstructing the dome model when the earthquake distribution is not ideal, we took subsets of our data for 15 incident plane waves coming only from the left or right (Fig. 9 lower panels, again with a dense receiver spacing of 1 km). Earthquakes from different directions (and their respective receiver functions) will image parts of the crustal model differently, depending on the local angle of incidence. *P* waves that are incident almost perpendicularly on Moho structures produce very small *PS* conversions and therefore do not contribute to the crustal image. To study crustal structures with signals of 1 Hz and with a good earthquake distribution, an average station spacing of less the 5 km is necessary when post-stack migration is applied to obtain a high-resolution image. These parameters are scalable; that is, when using lower signal frequencies one can increase the average station spacing, but has to accept decreased spatial resolution. Whilst most previous experiments do not fulfil the requirements (station density, signal frequencies, etc.), recent and future investigations (Eifel plume experiment, Ritter *et al.* 1998) with larger apertures and instrument numbers and higher station density will give data sets suitable for crustal imaging by RF migration.

Standard procedures such as binning, NMO corrections, stacking and post-stack depth migration with RF data will result in reasonable crustal images. Of course, the spatial resolution will be decreased due to the lower signal frequencies. When processing observed data one can take advantage of the existing analytical processing tools, NMO and migration velocity analysis tools. Several static tools can be used to control

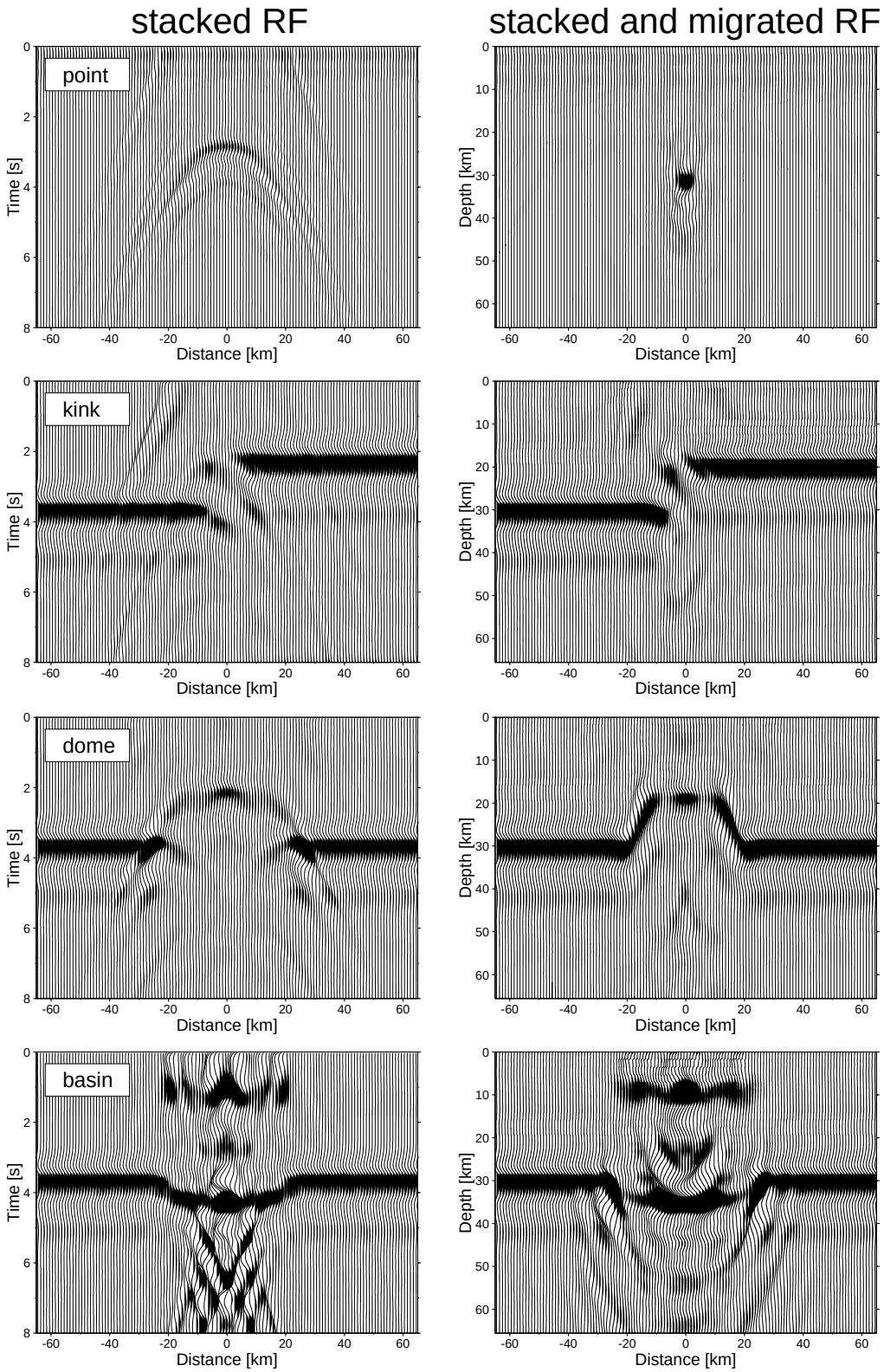

Figure 7. Moveout-corrected and stacked data for models (a), (b), (c) and (d) of Fig. 4 (left) and their depth-migrated versions (right) for 30 earthquakes, 15 from each direction. Note the substantial improvement of the spatial resolution and the reduction of the diffraction artefacts, especially for the low-velocity basin model (apparent Moho depression, sub-Moho structures).

time delays (elevation, velocity and residual statics) to enhance the signal-to-noise ratio. More complicated (realistic) models and observed data will, of course, need pre-stack migration techniques to be applied to the high-quality and dense data to obtain reliable crustal images. All suggested processing steps can be easily adapted to 2-D data sets (2-D station distribution). Generally, the extension to process RF data for deeper boundaries and structures is straightforward as long

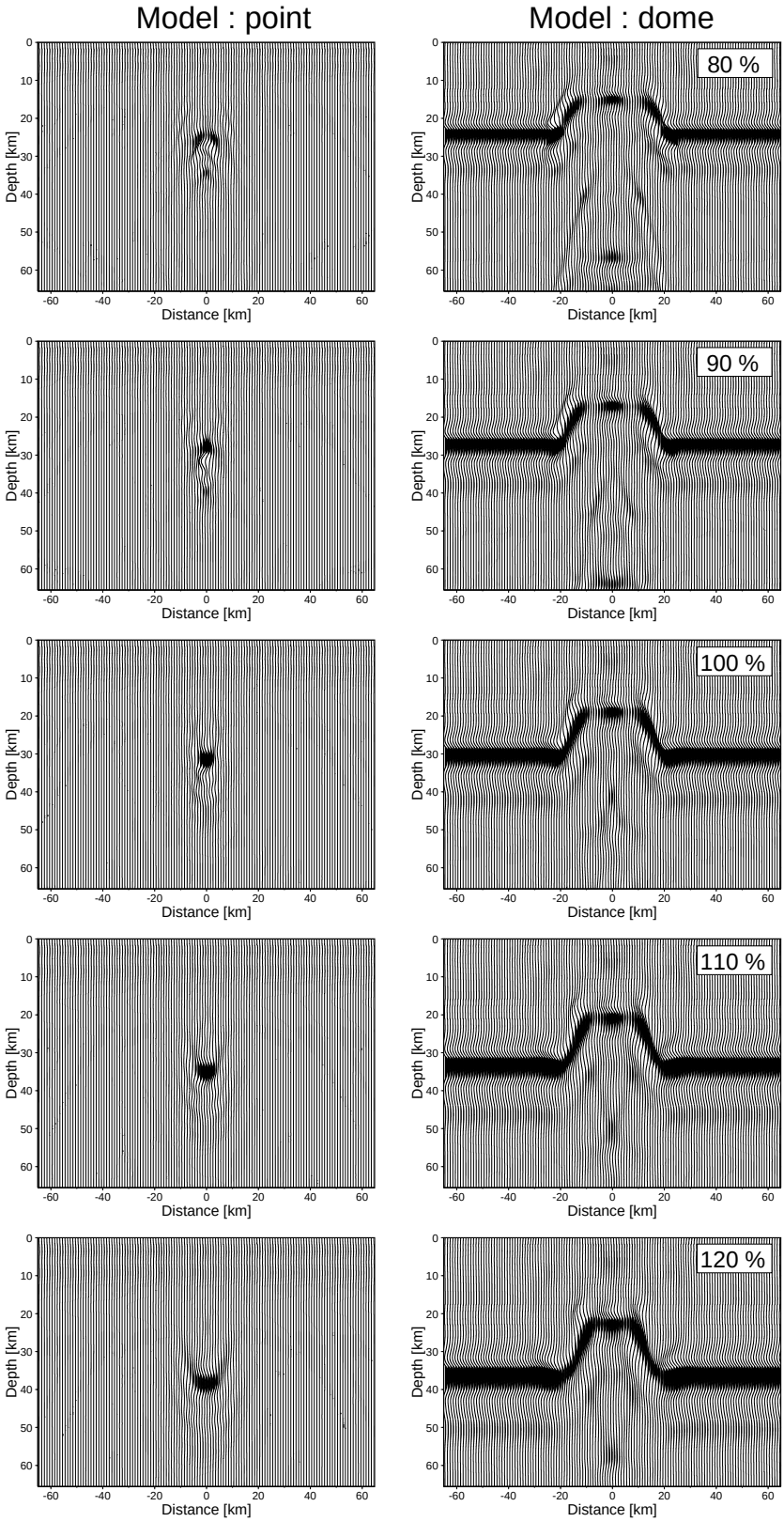

Figure 8. Test of migration velocities given in per cent relative to the correct velocities for model (a) (left) and (c) (right). Velocities that differ from the correct values by more than 10 per cent tend to degrade the migration results.

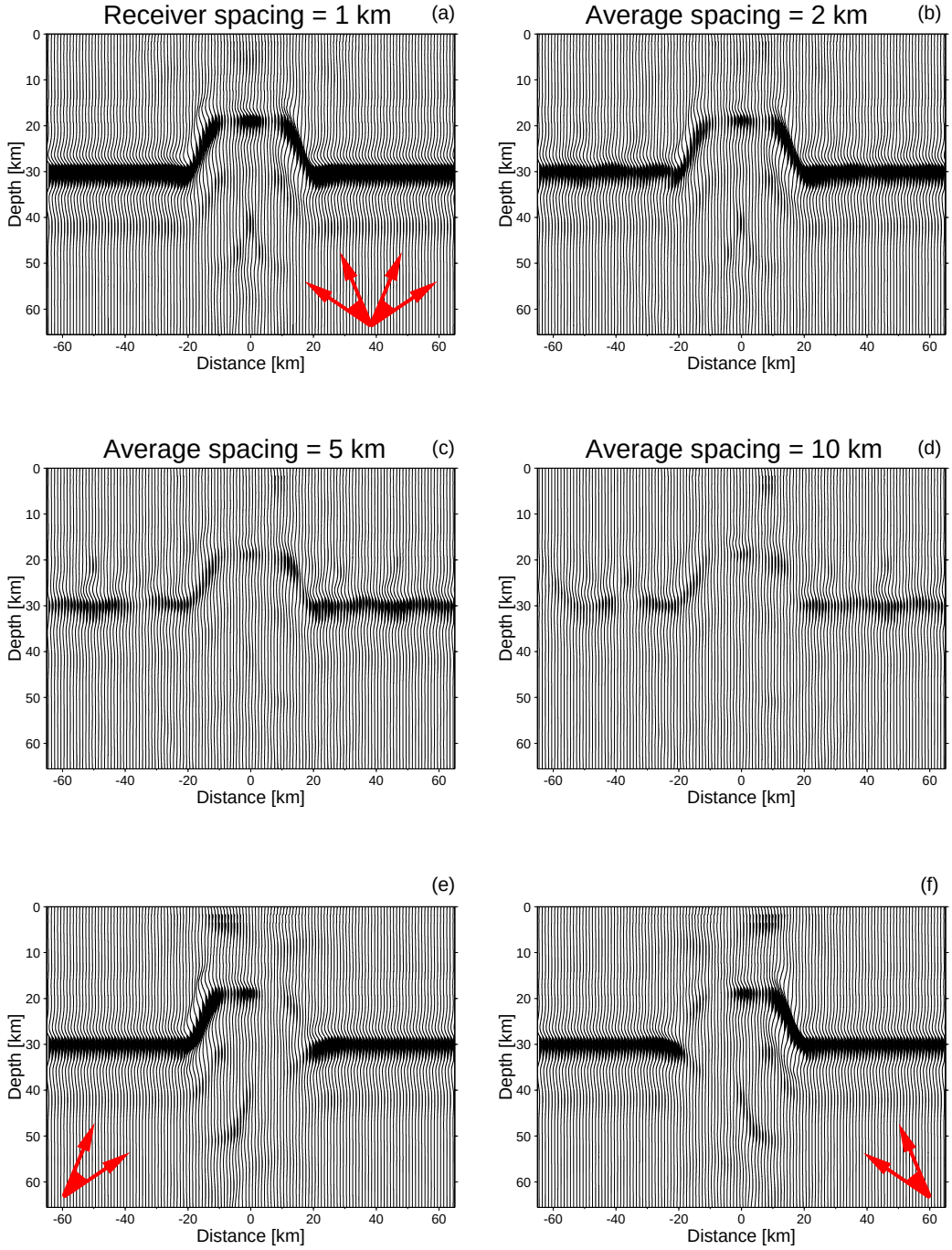

Figure 9. To test the influence of the station density and the distribution at the surface, we reconstructed the dome model (including stacking and depth migration) for several data subsets. A random distribution of receivers with average spacings of 2, 5 and 10 km was assumed (b, c and d) and compared with the 1 km spaced data (a). Receiver spacings of more than 5 km result in poor images of the input model. Note the decrease of the S/N ratio and the discontinuous character of the boundaries for larger receiver spacings. (e) and (f) demonstrate the selective imaging capabilities (apparent gap in dome structure) when an asymmetric distribution of earthquakes (events only from the left, e, or events only from the right, f) occurs.

as attention is paid to the non-planar character of the wave fronts, the sphericity of the Earth and the curvature of the ray path. As for near-vertical seismic processing, absolute depth determinations to boundaries are problematic owing to the velocities not being very well known, and the principal problem of their estimation due to small and therefore non-sensitive moveouts.

6 CONCLUSIONS

With the transition from sparse and irregular distributions of seismic stations to dense and regular arrays, the RFM can be used to image crustal structures. The resolving power of the RFM is not only increased by the improvement of the signal-to-noise ratio due to stacking, but is significantly increased

by migration, and therefore could supplement standard near-vertical seismic studies (see also Gossler *et al.* 1999). We propose a data processing approach that is equivalent to and takes advantage of the standard seismic data processing techniques routinely used in the exploration industry. To test its capabilities and effectiveness, seismic processing steps were applied to synthetic data derived by the finite difference method for several simple crustal models. Binning, NMO corrections, stacking and depth migration are capable of reconstructing the models with sufficiently high spatial resolution. The power and necessity of migration can be seen in Fig. 7. Without migration, structural interpretation of the RFM images seems to be prone to misinterpretation and the stacked but not migrated image 'suffers' from a relatively low horizontal spatial resolution, as expected from the corresponding Fresnel zones. We also demonstrate that sufficiently dense (<5 km at 1 Hz) and properly distributed earthquakes and receivers are essential to image crustal structure adequately. A point of warning concerns the effects that near-surface or shallow low-velocity structure will have on the imaging capabilities of the receiver function method (see Fig. 7d). This problem could be overcome by developing a migration scheme, which simultaneously migrates not only the *PS* energy but also its *PP*, *PPS*, *PSS*, etc., counterparts.

To extend the migration approach to deeper structures, for instance the upper mantle discontinuities at 410 and 660 km depth, effects that are caused by the sphericity of the Earth, the non-planar wave fronts and the ray path curvature have to be taken into account. In the case of the rather complicated crustal structures that are present in many experiments, pre-stack migration of the data has to be applied. Data sets with a 2-D distribution of seismic stations such as in the Eifel plume experiment (Ritter *et al.* 1998) can in the future be processed with a similar approach by extending the suggested processing steps to their 3-D versions.

ACKNOWLEDGMENTS

The authors are grateful to R. Kind, G. Bock and M. Stiller for numerous discussions on receiver functions and migration techniques. We thank J. Mechie for helpful reviews of earlier drafts of this manuscript. We also appreciate suggestions and comments made by G. Müller and two anonymous referees. The numerical calculations of the synthetic seismograms were supported by the High-Performance Computer Centers in Stuttgart and Jülich and were carried out on their Cray T3E. All figures were generated using the GMT software of Wessel & Smith (1991).

REFERENCES

Birch, F., 1961. The velocity of compressional waves in rocks to 10 kilobars, part 2, *J. geophys. Res.,* **66,** 2199–2224.

Bostock, M.G., 1998. Mantle stratigraphy and evolution of the Slave province, *J. geophys. Res.,* **103,** 21 183–21 200.

Bostock, M.G. & Rondenay, S., 1999. Migration of scattered teleseismic body waves, *Geophys. J. Int.,* **137,** 732–746.

Burdick, L.J. & Langston, C.A., 1977. Modeling crustal-structure through the use of converted phases in teleseismic body-waveforms, *Bull. seism. Soc. Am.,* **67,** 677–691.

Dueker, K.G. & Sheehan, A.F., 1997. Mantle discontinuity structure from midpoint stacks of converted *P* to *S* waves across the Yellowstone hotspot track, *J. geophys. Res.,* **102,** 8313–8327.

Dueker, K.G. & Sheehan, A.F., 1998. Mantle discontinuity structure beneath the Colorado Rocky Mountains and High Plains, *J. geophys. Res.,* **103,** 7153–7169.

Gossler, J., Kind, R., Wylegalla, K., Sobolev, S., Kämpf, H., Wyllegalla, K. & Stiller, M., 1999. Major crustal features from the Harz Mountains and the Baltic Shield derived from receiver functions, *Tectonophysics,* **314,** 321–333.

Gurrola, H. & Minster, J.B., 1998. Thickness estimates of the upper-mantle transition zone from bootstrapped velocity spectrum stacks of receiver functions, *Geophys. J. Int.,* **133,** 31–43.

Gurrola, H., Minster, J.B. & Owens, T., 1994. The use of velocity spectrum for stacking receiver functions and imaging upper mantle discontinuities, *Geophys. J. Int.,* **117,** 427–440.

Hedlin, M.A., Minster, B.J. & Orcutt, J.A., 1994. Resolution of prominent crustal scatterers near the NORESS small-aperture array, *Geophys. J. Int.,* **119,** 101–115.

Jones, C.H. & Phinney, R.A., 1998. Seismic structure of the lithosphere from teleseismic converted arrivals observed at small arrays in the southern Sierra Nevada and vicinity, California, *J. geophys. Res.,* **103,** 10 065–10 090.

Kelly, K.R., Ward, R.W., Treitel, S. & Alford, R.M., 1976. Synthetic seismograms: a finite-difference approach, *Geophysics,* **41,** 2–27.

Kennett, B.L.N. & Engdahl, E.R., 1991. Traveltimes for global earthquake location and phase identification, *Geophys. J. Int.,* **105,** 429–465.

Kosarev, G., Kind, R., Sobolev, S.V., Yuan, X., Hanka, W. & Oreshin, S., 1999. Seismic evidence for a detached Indian lithospheric mantle beneath Tibet, *Science,* **283,** 1306–1309.

Langston, C.A., 1977. Corvallis, Oregon, crustal and upper mantle receiver structure from teleseismic *P* and *S* waves, *Bull. seism. Soc. Am.,* **67,** 713–724.

Langston, C.A., 1979. Structure under Mount Rainier, Washington, inferred from teleseismic body waves, *J. geophys. Res.,* **84,** 4749–4762.

Levander, C.A. & Hill, N.R., 1985. P-SV resonances in irregular low-velocity surface layers, *Bull. seism. Soc. Am.,* **75,** 847–864.

Peng, X. & Humphreys, E.D., 1998. Crustal velocity structure across the eastern Snake River Plain and Yellowstone swell, *J. geophys. Res.,* **103,** 7171–7186.

Revenaugh, J., 1995. A scattered-wave image of subduction beneath the Transverse Ranges, *Science,* **268,** 1888–1892.

Ritter, J.R.R., Christensen, U., Achauer, U., Bahr, K. & Weber, M., 1998. Search for a mantle plume under Central Europe, *EOS, Trans. Am. geophys. Un.,* **79,** 420.

Saunders, P., Priestley, K. & Taymaz, T., 1998. Variations in the crustal structure beneath western Turkey, *Geophys. J. Int.,* **134,** 373–389.

Sheriff, R.E. & Geldart, L.P., 1995. *Exploration Seismology,* Cambridge University Press, Cambridge.

Vinnik, L.P., 1977. Detection of waves converted from *P* to *SV* in the mantle, *Phys. Earth planet. Inter.,* **15,** 39–45.

Wessel, P. & Smith, W., 1991. Free software helps map and display data, *EOS, Trans. Am. geophys. Un.,* **72,** 441, 445–446.

Wu, R. & Aki, K., 1985. Scattering characteristics of elastic waves by an elastic heterogeneity, *Geophysics,* **50,** 582–595.

Yilmaz, O., 1987. *Seismic Data Processing,* Society of Exploration Geophysicists, Tulsa, OK.

Yuan, X., Ni, J., Kind, R., Mechie, J. & Sandvol, E., 1997. Lithospheric and upper mantle structure of southern Tibet from a seismological passive source experiment, *J. geophys. Res.,* **102,** 27 491–27 500.